Journal of Engineering Science and Technology
Vol. 14, No. 3 (2019) 1374 - 1397

DECOUPLED INTEGRAL LQR CONTROLLER WITH ANTI-WINDUP COMPENSATOR FOR MIMO TWO ROTOR AERODYNAMICAL SYSTEM (TRAS)

SAEED AL-HADDAD, HERMAN WAHID*

School of Electrical Engineering, Faculty of Engineering,
Universiti Teknologi Malaysia, 81310 UTM Skudai, Johor, Malaysia
*Corresponding Author: herman@fke.utm.my

Abstract

This paper employs a design of two sub-controllers based on a Linear Quadratic Regulator (LQR) for Two Rotor Aero-dynamical System (TRAS) in two Degree of Freedom (2-DOF) motion. TRAS is a nonlinear Multi-Input Multi-Output (MIMO) system that resembles the behaviour of a helicopter in certain aspects. The main focus of the research work is to control and stabilize the TRAS system in 2-DOF so that the desired trajectory is tracked quickly and accurately even in the presence of disturbances. However, this not always possible due to some reasons such as the strong cross couplings, poorly tuned control parameters and integral windup phenomena that significantly deteriorate the transient response. In this work, TRAS is decoupled into two subsystems (horizontal and vertical) with the cross couplings considered as disturbances. The derivation of the linear model of each subsystem is developed using Jacobean linearisation matrix. An optimal LQR controller is designed and tuned using Particle Swarm Optimisation (PSO) algorithm for each subsystem. To get full state information, provide asymptotic tracking for the reference signal and alleviate integral windup phenomena each sub-LQR controller has been combined with full state observer, integral action gain and anti-windup compensator based on back-calculation technique, respectively to ensure fast and reliable control of TRAS system without degrading the transient response. Experimental results show that the Decoupled Integral LQR Controller (DILQRC) exhibits a better performance in terms of transient and steady state responses with significant reduction of settling time, overshoot percentage and error index it also produces less aggressive and smooth control signals as compared to the Cross Coupled PID Controller (CCPIDC) tuned by the manufacturer.

Keywords: Anti-windup, Back-calculation, Full state observer, Integral action, Linear Quadratic Regulator (LQR), Particle Swarm Optimisation (PSO), Two rotor aerodynamical system (TRAS).

1. Introduction

Control of Two Rotor Aerodynamical System (TRAS) has become one of the most challenging engineering tasks due to the complicated nonlinear interaction and significant cross-couplings between the horizontal and vertical planes. Furthermore, some state variables are not accessible for measurement.

Since TRAS is considered as multi-input multi-output (MIMO) system with significant cross couplings, one of the early approaches to multivariable control is decoupling control [1]. The interaction in a MIMO system makes control and stability analysis of the system very complicated compared to that of a Single Input Single Output (SISO) system [2].

The feedback control systems are extensively used in automobile and military hardware applications to increase efficiency and reliability, as these control systems are being required to deliver more accurate and better overall performance in the face of difficult and complicated application conditions. However, to meet the demands of improved performance and robustness, control engineers will require new design techniques and better underlying theory [3].

Most of the controllers such as Proportional Integral Derivative (PID), Linear Quadratic Regulator (LQR) and Model Predictive Control (MPC) contain tuning parameters that define the behaviour of the controller. However, the tuning of these parameters using classical approaches such as trial and error is a tedious practice and does not guarantee the desired performance [4]. In order to have an optimal control system, the parameters of the controller should be tuned properly and carefully [5].

From the above, we can conclude that the decoupling of TRAS is highly desired to simplify the control of such a complicated system .However, to achieve fast and reliable control of TRAS a feedback control system has to be designed and properly tuned with the addition of suitable techniques.

Fractional order PID controller using Nelder-Mead optimisation technique was able to minimise the cross coupling between the system planes also it required less control effort to stabilise the system as compared to other classical PID controllers [6]. On the other side, the system had a settling time of 9 seconds for the horizontal and vertical angles of the system as well as a high percentage of overshoot above 13% for both angles. Yang et al. [7] reported that a composite controller of active disturbance rejection and input shaping command has been investigated in simulation and real-time implementation. However, both angles of the system had a settling time of more than 6.3 seconds and 9.1 seconds in simulation and experimental results, respectively. Ahmad et al. [8] proposed the fixed structure H_∞ controller with the static linear decoupling method, which is found to be capable of handling the system effectively because of its simple structure and robust nature.

Al-Mahturi and Wahid [9] optimally tuned LQR controllers, which have shown good results to control and stabilise each plane of TRAS system with a magnificent reduction in settling time and overshoot percentage, but the controllers were only implemented in simulation for one degree of freedom (1-DOF) motion and the robustness of the system was not investigated. Optimal LQR controller with integral action gave better performance as compared to the sliding mode controller [10] and an optimal LQR controller is found to provide better performance with reduced control effort as compared to the classical PID controller [11].

Nevertheless, both studies showed that the system had a settling time above 5 seconds for both angles and no conclusions were drawn on the system robustness properties. Phillips and Sahin [10] explained that furthermore, the weight matrices of LQR were tuned manually, which do not give the optimal value. Similarly, Pandey and Laxmi [11] has chosen a random value of Q and R and varied them until the desired performance is met.

Wen and Lu [12] experimentally validated the use of robust deadbeat control technique for the twin rotor MIMO system (TRMS) in 2-DOF, however, the vertical angle took about 8 seconds to be settled with a small percentage of overshoot in the horizontal angle. Simulation and experimental results of multiple models with second level adaption controller showed improvement in transient and steady responses in comparison with single model adaptive controller [13]. However, the simulation results showed that the system settled in less than 7 seconds for both angles, meanwhile, that performance significantly degraded in the real-time implementation as the system took more than 12 seconds to be settled for both angles with 35.6% of overshoot in the vertical angle.

A multivariable integral sliding mode controller has been used to track both the azimuth and pitch angles of the system and it showed excellent tracking behaviour for both angles with small errors [14]. Detescu et al. [15] proposed that a nonlinear MPC with extended Kalman filter is validated experimentally to have superior performance as compared to multivariable PID controller, in spite of that, the tuning of a large number of MPC parameters was the most time-consuming problem in this study. Raghavan and Thomas [16] reported that the MIMO MPC is found to be capable of handling the cross coupling between the system parameters while rejecting disturbances and maintains robustness to the system. However, the system was able to track the reference trajectories with a settling time less than 20 seconds and a percentage of overshoot less than 7.5% for both angles. Moreover, the system was subjected to a number of oscillations due to the gravity effect.

It can be summarised that the control of TRAS system is divided into two main categories: the linear and nonlinear controllers. According to Raptis and Valavanis [17], the linear controllers have a simple structure and lower computational cost but they are suffering from long settling time and a higher percentage of overshoot, moreover, some of the linear controllers, which involve integral action gain as stated by Phillips and Sahin [10] and Pandey, and Laxmi, [11] are designed without taking into account the nonlinearity of the actuators which causes integral windup phenomena that significantly deteriorate the transient response. On the other hand, the nonlinear controllers have superior performance and robust nature, but they involve a higher computational cost and difficulties in real time implementation [17], especially those who are involved adaption laws that significantly increase the computational load and deteriorate the transient response when the adaption is initiated [18].

In this work, TRAS is decoupled into two subsystems (horizontal and vertical) with the cross couplings considered as disturbances. The derivation of the linear model of each subsystem is developed using Jacobean linearisation matrix. Optimal state feedback LQR controller is designed and tuned using particle swarm optimisation (PSO) algorithm for each subsystem. In order to achieve fast and reliable control of TRAS system in 2-DOF even in the presence of disturbances and significant cross couplings, each sub-LQR controller has been

combined with full state observer, integral action gain and an anti-integral windup compensator to improve the performance of each sub-LQR controller. The full state observer is used to get full information of all the states of the system since two state variables are not accessible for measurement in the TRAS system, namely azimuth angular velocity and pitch angular velocity. The addition of integral action gain to each sub-LQR controller provides zero steady-state error in the output of the system [19]. However, an inherent drawback of the use of integral action gain is the integral windup phenomenon, which occurs when the controller generates a control signal that exceeds the limitation of the actuator, which significantly deteriorates the control system performance causing large, overshoot and slow settling time [20]. To alleviate integral windup phenomena effect, an anti-integral windup compensator based on back calculation technique has been added to each sub-LQR controller.

The evaluation of the designed decoupled integral LQR controller (DILQRC) is based on set point tracking and disturbance rejection and in order to provide a point of comparison the performance of the DILQRC is compared to the existing cross-coupled PID controller (CCPIDC) tuned by the manufacturer.

This paper tries to address that well designed and tuned optimal sub-LQR controllers combined with suitable techniques, namely integral action gain, full state observer and anti-integral windup compensator can be used to successfully control and stabilize a nonlinear and complicated system such as TRAS quickly and accurately providing fast settling time and small percentage of overshoot as compared to other controller design techniques presented in the literature.

The remainder of this paper is organised as follows: Section 2 describes the linear and nonlinear models of TRAS system. In Section 3, an optimal LQR controller with integral action is presented. The principles of the PSO algorithm are illustrated in Section 4, followed by the design of the full state observer in Section 5. Section 6 shows the design of an anti-integral windup technique based on back-calculation. Stability analysis of closed loop subsystems is carried out in Section 7. Experimental results are deliberated in Sections 8, followed by the conclusions in Section 9.

2. TRAS Description and Modelling

TRAS is a multivariable system that has two inputs and two outputs with significant interaction between its parameters. TRAS is a laboratory setup that is used to test and validate various flight control methods, as it resembles the behaviour of a helicopter in certain aspects as shown in Fig. 1.

An approximate Newtonian mathematical model of the TRAS is obtained by using Newton's second law of motion with the description and values of the physical parameters provided in Table 1 [21]. However, numerous previous works intensively debated on the mathematical modelling of TRMS (a variant of the TRAS). Based on studies by Rahideh and Shaheed [22] and Rahideh et al. [23], the Newtonian and Lagrangian methods for TRMS modelling has been discussed in which, dynamic modelling of TRMS using analytical and empirical approaches has been addressed. Tastemiro et al. [24] investigated recently, in a more complete dynamic modelling of TRMS using Euler–Lagrange method with experimental validation.

Table 1. Parameters definition of TRAS by INTECO [21].

Symbol	Description	Value
A_1	Mechanical constant	0.0947
a_1	Mechanical constant	3.3×10^{-6}
a_2	Mechanical constant	9.28×10^{-6}
B_1	Mechanical constant	0.04465
C_1	Mechanical constant	9.54136×10^{-3}
g	Gravitational acceleration	9.81 ms^{-2}
I_h	Moment of inertia for the tail rotor	2.7027×10^{-5} kgm^2
I_v	Moment of inertia for the main rotor	1.64×10^{-4} kgm^2
J_h	Moment of inertia with respect to vertical axis	0.02683 kgm^2
J_v	Moment of inertia with respect to horizontal axis	0.0300571 kgm^2
k_h	Friction constant of the tail propeller	0.00589
k_v	Friction constant of the main propeller	0.01271
l_m	Length of the main rotor	0.202 m
l_t	Length of the tail rotor	0.216 m

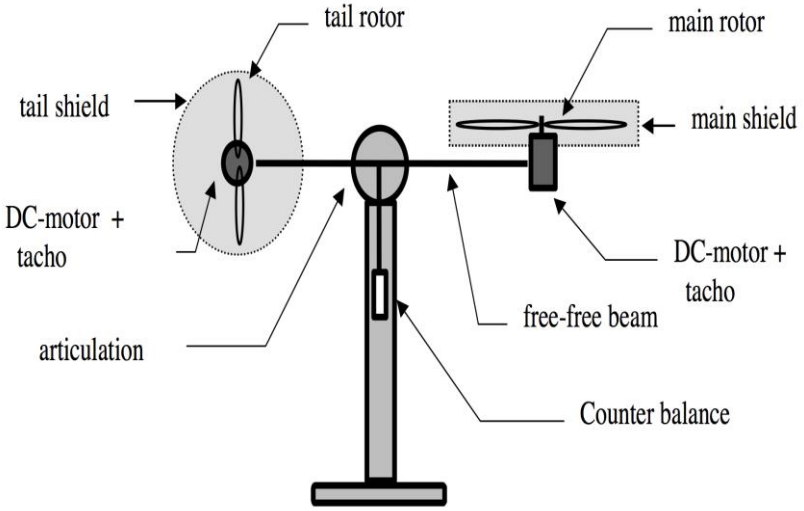

Fig. 1. TRAS system [21].

In a typical helicopter, the aerodynamic force is controlled by changing the angle of attack of the blades while in a laboratory setup, it is constructed such that the angle of attack of the blades is fixed and the controlling is done by varying the rotational speed of the rotors.

The TRAS consists of two rotors, which are the main and tail rotors. Both rotors are driven by two direct current motors, the main rotor is used to control the vertical motion (pitch angle) and the tail rotor is used to control the horizontal motion (azimuth angle). Two counterbalance levers attached with a weight at their ends are fixed to the beam at the pivot that determines the steady-state pitch angle [21].

2.1. Nonlinear models

The mathematical modelling of the decoupled horizontal plane can be written as in Eqs. (1) to (3) [21]:

$$\dot{x}_1 = \frac{1}{J_h} x_2 \tag{1}$$

$$\dot{x}_2 = \frac{l_t F_h(x_3)}{I_h} - \frac{k_h}{J_h} x_2 + \frac{a_1}{J_h \times I_h} x_2 \mid x_3 \mid \tag{2}$$

$$\dot{x}_3 = u_h - \frac{u_h(x_3)}{I_h} \tag{3}$$

where:

$$\begin{aligned} F_h(x_3) \cong \; & -4.869 \times 10^{-20} x_3^5 - 5.035 \times 10^{-17} x_3^4 + 4.64 \times 10^{-12} x_3^3 \\ & +7.562 \times 10^{-9} x_3^2 + 2.435 \times 10^{-5} x_3 - 0.003716 \end{aligned} \tag{4}$$

$$\begin{aligned} u_h(x_3) \cong \; & -1.08 \times 10^{-20} x_3^5 + 5.25 \times 10^{-18} x_3^4 + 1.43 \times 10^{-12} x_3^3 \\ & -8.13 \times 10^{-10} x_3^2 + 0.0001534 x_3 + 0.002067 \end{aligned} \tag{5}$$

where: x_1 is the azimuth angle, x_2 is the azimuth angular velocity, x_3 is the rotational speed of the tail rotor, u_h is the control input to the tail rotor, $F_h(x_3)$ is a nonlinear relationship between the rotational speed of the tail rotor and horizontal thrust and $u_h(x_3)$ is a nonlinear relationship between the rotational speed of the tail rotor and the control input to the tail rotor.

The mathematical modelling of the decoupled vertical plane can be written as in Eqs. (6) to and (8) [21]:

$$\dot{x}_4 = \frac{1}{J_v} x_5 \tag{6}$$

$$\dot{x}_5 = \frac{l_m F_v(x_6)}{I_v} - \frac{k_v}{J_v} x_5 - \frac{a_2 k_v}{J_v \times I_v} x_5 \mid x_6 \mid + g((A_1 - B_1)\cos x_4 + C_1 \sin x_4 \tag{7}$$

$$\dot{x}_6 = u_v - \frac{u_v(x_6)}{I_v} \tag{8}$$

where:

$$\begin{aligned} F_v(x_6) \cong \; & -1.345 \times 10^{-18} x_6^5 - 5.221 \times 10^{-16} x_6^4 + 3.513 \times 10^{-11} x_6^3 \\ & +2.17 \times 10^{-18} x_6^2 + 0.0002012 x_6 - 0.01453 \end{aligned} \tag{9}$$

$$\begin{aligned} u_v(x_6) \cong \; & -1.1 \times 10^{-18} x_6^5 + 1.522 \times 10^{-16} x_6^4 - 8.796 \times 10^{-12} x_6^3 \\ & -1.46 \times 10^{-9} x_6^2 + 0.00021664 x_6 - 0.003139 \end{aligned} \tag{10}$$

where: x_4 is the pitch angle, x_5 is the pitch angular velocity, x_6 is the rotational speed of the main rotor, u_v is the control input to the main rotor, $F_v(x_6)$ is a nonlinear relationship between the rotational speed of the main rotor and vertical thrust and $u_v(x_6)$ is a nonlinear relationship between the rotational speed of the main rotor and the control input to the main rotor.

2.2. Linear models

The LQR controller is a linear state feedback controller, which requires a linear model to be implemented, thus, each nonlinear subsystem is linearised using Jacobean linearisation matrix around the equilibrium point (x, u) at $(0,0)$ [25]. Where x is the

states of each subsystem and u is the control input. The A and B Jacobean linearisation matrices for each subsystem can be evaluated as follows [25]:

$$A = \frac{\partial f}{\partial x}\Big|_{x=0,u=0} ; B = \frac{\partial f}{\partial u}\Big|_{x=0,u=0}$$

where: f is the differential equation of each state.

The linear model of each subsystem can be obtained by evaluating the Jacobean linearisation matrices, choosing the azimuth and pitch angles as the output states for the C matrix of the horizontal and vertical subsystems, respectively and assumes zero feedforward D matrix for each subsystem.

The linear model of the decoupled horizontal plane can be written in state space form as in Eq. (11):

$$\begin{aligned} \begin{bmatrix} \dot{x}_1 \\ \dot{x}_2 \\ \dot{x}_3 \end{bmatrix} &= \begin{bmatrix} 0 & 37.27 & 0 \\ 0 & -0.22 & 0.195 \\ 0 & 0 & -5.68 \end{bmatrix} \begin{bmatrix} x_1 \\ x_2 \\ x_3 \end{bmatrix} + \begin{bmatrix} 0 \\ 0 \\ 1 \end{bmatrix} [u_h] \\ y_h &= \begin{bmatrix} 1 & 0 & 0 \end{bmatrix} \begin{bmatrix} x_1 \\ x_2 \\ x_3 \end{bmatrix} + [0][u_h] \end{aligned} \tag{11}$$

The linear model of the decoupled vertical plane can be written in state space form as in Eq. (12):

$$\begin{aligned} \begin{bmatrix} \dot{x}_4 \\ \dot{x}_5 \\ \dot{x}_6 \end{bmatrix} &= \begin{bmatrix} 0 & 33.27 & 0 \\ -0.10 & -0.42 & 0.25 \\ 0 & 0 & -1.42 \end{bmatrix} \begin{bmatrix} x_4 \\ x_5 \\ x_6 \end{bmatrix} + \begin{bmatrix} 0 \\ 0 \\ 1 \end{bmatrix} [u_v] \\ y_v &= \begin{bmatrix} 1 & 0 & 0 \end{bmatrix} \begin{bmatrix} x_4 \\ x_5 \\ x_6 \end{bmatrix} + [0][u_v] \end{aligned} \tag{12}$$

3. LQR Controller with Integral Action

By considering a linear time-invariant system, the state and output equations with control input can be written as in Eq. (13) [26]:

$$\begin{aligned} \dot{x} &= Ax + Bu \\ y &= Cx \end{aligned} \tag{13}$$

The conventional LQR design problem is to minimise the following quadratic performance index function as in Eq. (14) [27]:

$$J = \int_0^\infty (x^T Q x + u^T R u)\, dt \tag{14}$$

The control input here is linear and the control penalty is given by $(u^T R u)$ where $R \in \Re^{m \times m}$ is the square positive definite matrix. The state penalty is expressed as $(x^T Q x)$ where $Q \in \Re^{n \times n}$ is a positive semi-definite matrix. The control value u is representing the optimal control input, which is given by Eq. (15) [27]:

$$u(t) = -Kx(t) = -R^{-1} B^T P x(t) \tag{15}$$

The matrix K is determined to minimise the performance index. Here, P is the solution of the Riccati equation, and K is the linear optimal feedback matrix. Riccati equation can be solved by Eq. (16) [27]:

$$PA + A^T P - PBR^{-1}B^T P + Q = 0 \tag{16}$$

The Q and R matrices plays an important role on the overall system performance, thus, they should be chosen appropriately.

By adding an integral action, a new state that is multi-dimensional will be added to the original states of the system [26]. According to Nise [26], the system has the state vector $[x \quad x_a]^T$, where x_a is the new integral state:

$$\dot{x}_a = r - y = r - Cx \tag{17}$$

$$= [-K \quad K_e]\begin{bmatrix} x \\ x_a \end{bmatrix} \tag{18}$$

where: r is the reference signal and K_e is the integral action gain.

By substituting Eqs. (17) and (18) in Eqs. (15) and (16) yields [26]:

$$\begin{aligned} \begin{bmatrix} \dot{x} \\ \dot{x}_a \end{bmatrix} &= \begin{bmatrix} A - BK & BK_e \\ -C & 0 \end{bmatrix}\begin{bmatrix} x \\ x_a \end{bmatrix} + \begin{bmatrix} 0 \\ 1 \end{bmatrix} r \\ y &= [C \quad 0]\begin{bmatrix} x \\ x_a \end{bmatrix} \end{aligned} \tag{19}$$

The state space representation of the state feedback control with integral action is shown in Eq. (19). By choosing appropriate state feedback gain and integral action gain that makes the system asymptotically stable, the system output will accurately track the reference signal [25].

4. Particle Swarm Optimisation (PSO)

PSO optimisation technique was originally inspired by the behaviour of fish swarms, as well as bees and other species [28]. The concept in this technique is to look for the best solution among the whole swarm for a specific cost function. PSO was introduced by James Kennedy and Russell Eberhart in (1995) and it is used as a powerful optimisation algorithm in many applications for its satisfactory results.

Implementing PSO is very simple as only two equations are required for the optimisation process: position equation and velocity equation. For each step in PSO, all particles will be initialised with a random position and velocity vectors and they will be evaluated to a cost function relevant to their position. Similar to most optimisation techniques finding Personal Best (x_{PB}) and Global Best (x_{GB}) for all particles in each iteration step will be calculated and the velocity and position vectors of each particle will be updated according to Eqs. (20) and (21), respectively [28]:

$$v_i(t+1) = w \times v_i(t) + c_1 \times r_1 \times \left(x_{PB} - x_i(t)\right) + c_2 \times r_2 \times \left(x_{GB} - x_i(t)\right) \tag{20}$$

$$x_i(t+1) = x_i(t) + v_i(t+1) \tag{21}$$

where w is the inertia weight factor, c_1 and c_2 are the personal acceleration coefficient and social acceleration coefficient, respectively and r_1 and r_2 are randomly distributed numbers between $(0,1)$. The parameter w makes the particles converge to the global best solution rather than oscillating around it. The parameters of PSO algorithm are provided in Table 2.

In this optimization technique, the value of the inertia weight factor is adjusted according to Eq. (22):

$$w = w \times w_{damp} \tag{22}$$

where w_{damp} is the damping ratio of the inertia coefficient.

According to INTECO [21], the optimisation purpose, a nonlinear 2-DOF TRAS model given is considered for the tuning of the Q and R matrices of each sub-LQR controller. Each optimisation process is carried out for 100 iterations. The cost function used in the tuning process is the minimisation of the settling time and the percentage of overshoot as in Eq. (23):

$$F = \text{ST+OV} \tag{23}$$

where: ST is the settling time and OV is the percentage of overshoot.

Based on the PSO algorithm, the complete parameters tuning steps for each sub-LQR controller can be summarised as follows:

- Step 1. Randomly generate an initial population of particles.
- Step 2. Calculate the cost function value of each particle.
- Step 3. For each particle, if the cost function value is better than x_{PB}, then set the present position as the new particle best. And if the cost function value is better than x_{GB}, then let this particle take the place of the x_{GB}. Otherwise, the present particle best and global best still remain.
- Step 4. Update the velocity and position of each particle according to Eq. (20) and Eq. (21). And then, update the inertia weight factor according to Eq. (22).
- Step 5. If the total number of iterations is achieved, stop the algorithm. Otherwise, go back to step 2.

Figure 2 shows the convergence of the cost function for each optimisation process. It can be noticed that the particles of PSO are able to find the best solution in almost forty number of iterations. Table 3 shows the results obtained from each optimisation process.

Table 2. Parameters of PSO.

Parameter	Value
Maximum number of iteration	100
Population size	50
Inertia weight coefficient (w)	1
Damping ratio of inertia weight coefficient (w_{damp})	0.99
Personal acceleration coefficient (c_1)	2
Social acceleration coefficient (c_2)	2

Table 3. Results of PSO for each sub-LQR controller parameter's tuning.

Sub-controller	Q matrix	R matrix
Horizontal	$\begin{bmatrix} 538.933 & 0 & 0 \\ 0 & 0 & 0 \\ 0 & 0 & 0 \end{bmatrix}$	$[0.94]$
Vertical	$\begin{bmatrix} 6097.30 & 0 & 0 \\ 0 & 0 & 0 \\ 0 & 0 & 0 \end{bmatrix}$	$[0.16]$

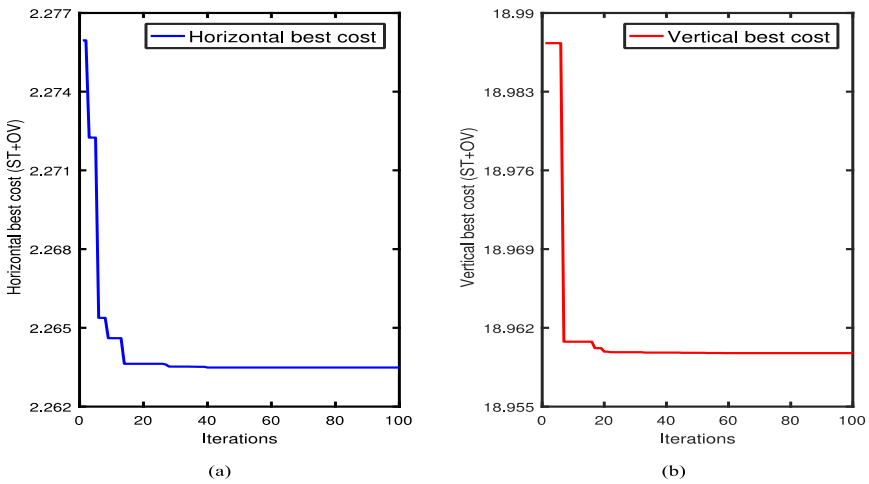

Fig. 2. Convergence of PSO cost function: (a) Horizontal controller best cost, (b) Vertical controller best cost.

5. Full State Observer

LQR controller requires that all states of the system are available for measurement [29]. For each subsystem, there are three state variables, whereas only two are accessible for measurement [21]. Thus, a full state observer is designed for each subsystem.

The mathematical model of the observer for linear time-invariant system can be defined as in Eq. (24) [29]:

$$\dot{\hat{x}} = A\,\hat{x} + Bu + K_e(y - C\,\hat{x}) \tag{24}$$

Since the system is controlled by the estimated feedback, the control input can be written as in Eq. (25):

$$u = -K\,\hat{x} + K_e x_a \tag{25}$$

The estimated states can be written as in Eq. (26):

$$\dot{\hat{x}} = A\,\hat{x} + B(-K\,\hat{x} + K_e x_a) + L(Cx - C\,\hat{x}) \tag{26}$$

and it can be arranged as in Eq. (27):

$$\dot{\hat{x}} = (A - LC - BK)\,\hat{x} + LCx + BK_e x_a \tag{27}$$

The inputs to the observer are the output y and the control input$u$. The gain L is called the observer gain and it is used as a correction for the model. Chosen of appropriate observer gain value determines how fast the error between the actual and estimated states will converge to zero [26]. As a rule of thumb, the observer poles determined by the matrix $(A - LC - BK)$ should be chosen to be two to five times faster than the controller poles to make sure that the error of the observer converges to zero very fast. However, if the output signal is contaminated by disturbances and measurement noises then the observer poles should be chosen to

be slower than the controller poles so that the bandwidth of the system will become lower and smooth the noise [29].

The horizontal observer poles are chosen to be five times faster than the horizontal controller poles. On the other side, the vertical observer poles are chosen to be four times slower than the vertical controller poles due to the vibrations that occur to the presence of rotor load, motor torque [30] and measurement noise, which result in a number of oscillations in the system response with long settling time.

To demonstrate the effect of the vertical observer poles selection on the overall vertical controller performance, the vertical plane is subjected to a sinusoidal signal with a measurement noise of a distributed random sequence with noise power of 0.1×10^{-0} as shown in Fig. 3. It can be clearly observed that the output of the vertical plane deviates significantly from the reference signal when the observer poles are five times faster than the controller poles, while in the case when the observer poles are four times slower than the controller poles the controller is able to smooth the noise and track the reference signal.

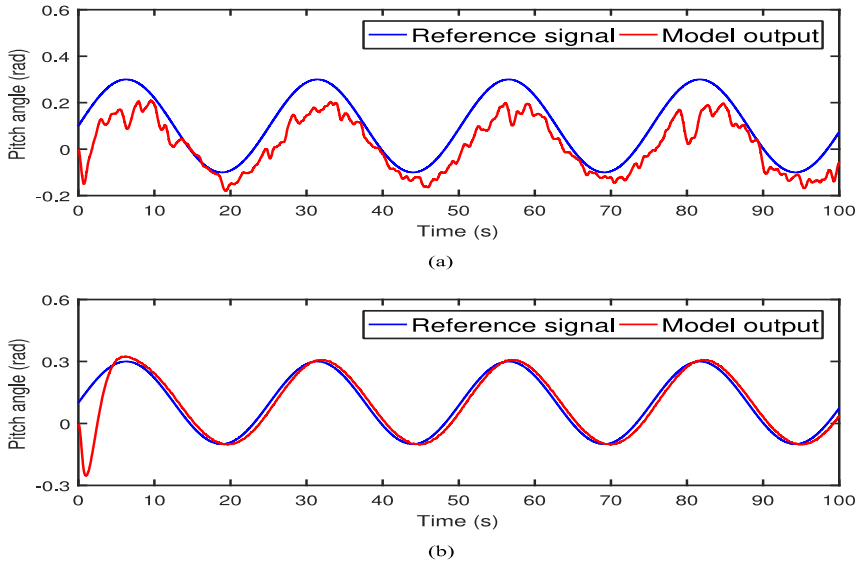

Fig. 3. Effect of observer poles selection on vertical controller performance: (a) Model output with five times faster observer poles, (b) Model output with four times slower observer poles.

The closed loop of each subsystem with state feedback controller, integral action gain and full state observer can be written in state space form as in Eq. (28):

$$\begin{bmatrix} \dot{x} \\ \dot{x}_a \\ \dot{\hat{x}} \end{bmatrix} = \begin{bmatrix} A & BK_e & -BK \\ -C & 0 & 0 \\ LC & BK_e & A - LC - BK \end{bmatrix} \begin{bmatrix} x \\ x_a \\ \hat{x} \end{bmatrix}$$
$$y = \begin{bmatrix} C & 0 & 0 \end{bmatrix} \begin{bmatrix} x \\ x_a \\ \hat{x} \end{bmatrix} \tag{28}$$

The overall performance of each controller is influenced by the eigenvalues of the state space in Eq. (28), thus, they should be placed appropriately to ensure the stability of the whole system.

6. Anti-integral Windup Compensator

In practice, all control loops and processes contain nonlinearities such as saturation in actuators. One of the most well-known phenomena in the control system is the integrator windup especially when the system starts up [31]. Back-calculation technique is based on recomputing the integral term when the controller reaches its limits. In particular, the integral value is increased or decreased by feeding the error signal produced from the difference between the saturated and unsaturated control signal to the integral action state [31].

Since the linear controller is designed to operate within a linear range, ignoring the actuator nonlinearities will cause the integrator to wind up, which will significantly deteriorate the closed loop performance. This performance deterioration is in the form of large overshoot and long settling time [32]. For the TRAS system the control signals of the main and tail motors are normalised and change in the range [-1,+1], which corresponds to a voltage range of [-24V,+24V].

In back-calculation technique, the difference between the saturated control signal and the unsaturated control signal is fed back to the integral action state, thus, the new integral action state can be written as follows:

$$\dot{x}_a = r - y + (\overline{u} - u) \tag{29}$$

$$\dot{x}_a = e + (\overline{u} - u) \tag{30}$$

where: e is the difference between the reference signal and the measured output.

The controller input for each subsystem with the addition of back-calculation is modified in the time domain as in Eq. (31):

$$u = -K\hat{x} + K_e \int_0^t \big(e + (\bar{u} - u)\big) dt \tag{31}$$

Rewriting the control input equation in the Laplace domain as follows:

$$u = -K\,\hat{x} + \frac{K_e}{s} e + \frac{K_e}{s} (\overline{u} - u) \tag{32}$$

$$\overline{u} = sat(u) \tag{33}$$

where the saturation function sat is defined as in Eqs. (33) and (34):

$$\overline{u} = \begin{cases} u_{min} & if \quad u < u_{min} \\ u & if \quad u_{min} \leq u \leq u_{max} \\ u_{max} & if \quad u > u_{max} \end{cases} \tag{34}$$

When the actuator saturates, the feedback signal $(\overline{u} - u)$ attempts to drive the error between the saturated and unsaturated control signals to zero by recomputing the integral action state such that the controller output is exactly at the saturation limit. When there is no saturation, the difference between $\overline{u}$ and u will be equal to zero, which breaks the feedback loop of back-calculation, in this case, the controller performs as in the standard mode ($\overline{u} = u$).

When the actuator saturates u is different from $\overline{u}$. Since the controller is not aware of the saturation in the actuator it computes the states as if the system input is u, therefore, state estimation errors can be further alleviated by feeding $\overline{u}$ to each observer instead of u [33]. The closed loop system under the proposed DILQRC with full state observer and back-calculation technique is depicted in Fig. 4.

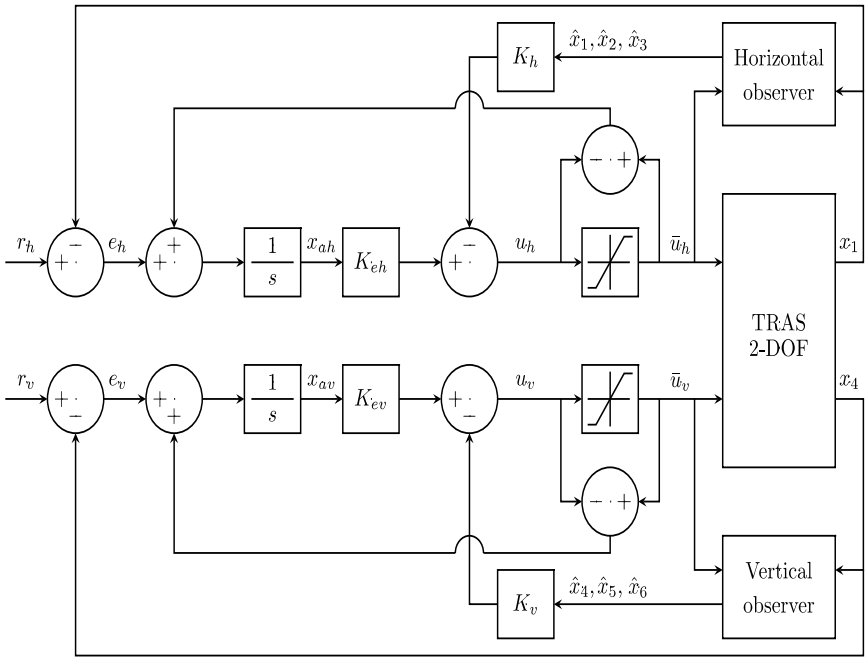

Fig. 4. TRAS with DILQRC combined with full state observer and back-calculation technique.

7. Stability Analysis of Closed Loop Subsystems

After the designing of the sub-LQR controllers combined with integral action gain, full state observer and back-calculation anti-integral windup technique, the closed loop analysis is carried out before the implementation on real 2-DOF TRAS system.

The frequency response of each closed loop subsystem with linear and nonlinear models is estimated using linear analysis tool in MATLAB/Simulink for the frequencies from 0.01 rad/s to 100 rad/s. Figure 5 shows the estimated frequency response of each closed loop subsystem. The average estimated bandwidths are approximately 1.43 rad/s and 1.35 rad/s for the horizontal and vertical closed loop subsystems, respectively. The vertical bandwidth is slightly lower than the horizontal bandwidth, this would yield the vertical sub-LQR controller to attenuate and smooth more exogenous disturbance or measurement noise signals that may enter the system. Both horizontal and vertical closed loop subsystems have a gain margin of approximately 14 dB and 15 dB, respectively and phase margin of roughly 175 and 151, respectively, which indicates that each closed loop subsystem is asymptotically stable.

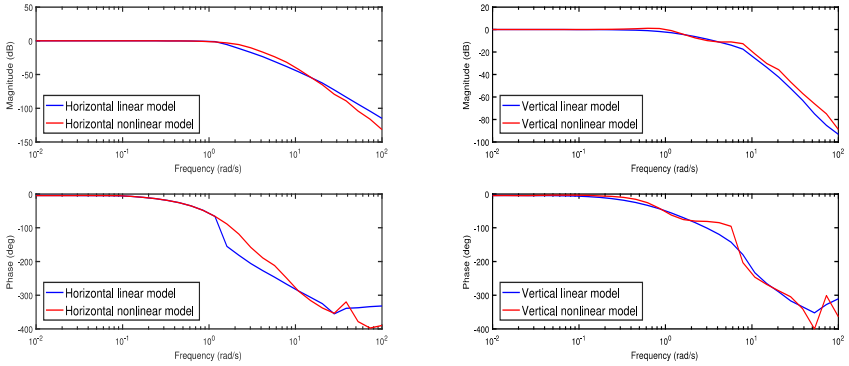

Fig. 5. Estimated frequency response of each closed loop subsystem: (a) Horizontal subsystem, (b) Vertical subsystem.

8. Experimental Results

The performance of the closed-loop system is depending on the transient response of the system, error, control and total variation indices. For assessing the transient response characteristic, the rise time (RT) is defined as the time it takes for the response to rise from 10% to 90% of the steady-state value, the settling time (ST) is defined as the time it takes for the response to fall within 5% of the steady-state value and the percentage of the overshoot (OV) as the maximum peak value of the response expressed as a percentage of the steady state value [29]. Error index is defined as the integrated absolute of error (IAE) between the reference signal and the controlled variable and is given as in Eq. (35) [34]:

$$\text{IAE} = \int_0^\infty | e(t) | \, dt \tag{35}$$

where: e(t) is the difference signal between the reference signal and the measured output signal.

The control index is defined as the integrated absolute control signal (IAC) that determines the amount of the control effort produced by the controller and is given as in Eq. (36) [34]:

$$\text{IAC} = \int_0^\infty | u(t) | \, dt \tag{36}$$

where: $u(t)$ is the control signal.

The Total Variation (TV) index characterise the smoothness of the control signal and input usage and is given as in Eq. (37) [13]:

$$\text{TV} = \sum_{m=1}^{n_s} | u_i(m+1) - u_i(m) | \tag{37}$$

where: n_s is the number of samples and $u_i(1), u_i(2), \ldots, u_i(n_s)$ is the discretised sequence of the input signals.

Lower error, control and total variation indices indicate accurate tracking for the reference signal, less control effort and less aggressive changes in the control signal, respectively. The closed-loop system is implemented in MATLAB/Simulink using ode5 solver with a fixed step size of 0.01 s.

The mechanical unit of TRAS is equipped with a dedicated I/O board and a power interface. The control computer communicates with the incremental sensors and motors interfaced by means of the dedicated I/O board. The I/O board is operated by real-time software within the MATLAB/Simulink environment [14, 21]. The experimental setup of TRAS is shown in Fig. 6.

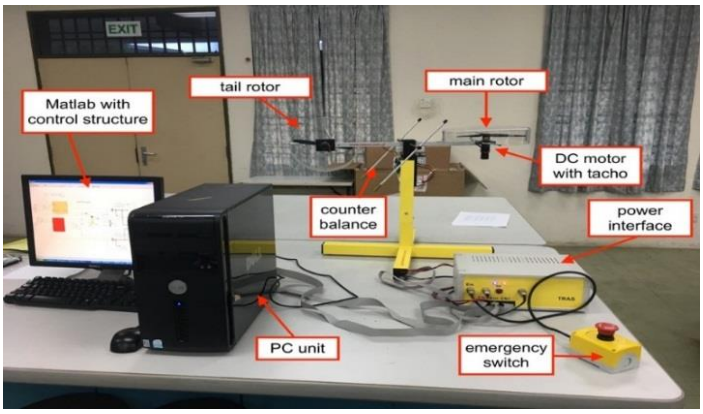

Fig. 6. TRAS experimental setup.

8.1. Setpoint tracking

For the step set point, tracking the system is subjected to step input of 0.8 rad in the horizontal plane and 0.3 rad in the vertical plane. Figure 7 shows the response of the TRAS system due to step input with both DILQRC and CCPIDC. Table 4 summaries the step reference performance characteristics of DILQRC and CCPIDC. For the horizontal plane, the DILQRC achieves better performance than the CCPIDC by reducing the rise time by 39.60% and the settling time by 46.49%. For the vertical plane, the CCPIDC has a better rise time than the DILQRC, but it takes 8.90 seconds to be settled, whereas the DILQRC takes only 2.60 seconds with a magnificent reduction in overshoot percentage from 62.09% to 1.24%.

Figure 8 shows the input control signals of DILQRC and CCPIDC due to a step input. The error, control and total variation indices of DILQRC and CCPIDC due to step input are summarised in Table 5. It can be clearly observed that the DILQRC significantly reduces the error index by 54.59% and 46.39% for horizontal and vertical planes, respectively indicating accurate tracking for the reference signals with less control effort and less aggressive changes in the control signals as compared to the CCPIDC.

Table 4. Step reference performance characteristics.

Controller	Plane	RT (s)	ST (s)	OV (%)
Pandey et al. [13] CCPIDC	Horizontal	2.02	3.42	0.00
	Vertical	1.08	8.90	62.09
DILQRC	Horizontal	1.22	1.83	0.48
	Vertical	2.16	2.60	1.24

Table 5. Error, control and total variation indices of DILQRC and CCPIDC due to step input.

Controller	Plane	IAE	IAC	TV
Pandey et al. [13] CCPIDC	Horizontal	1.96	7.29	201.52
	Vertical	0.97	10.86	87.58
DILQRC	Horizontal	0.89	6.34	145.52
	Vertical	0.52	10.81	16.93

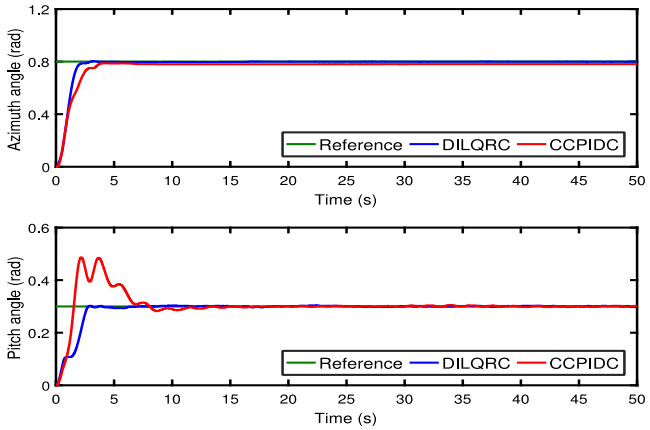

Fig. 7. Step input response of TRAS with DILQRC and CCPIDC.

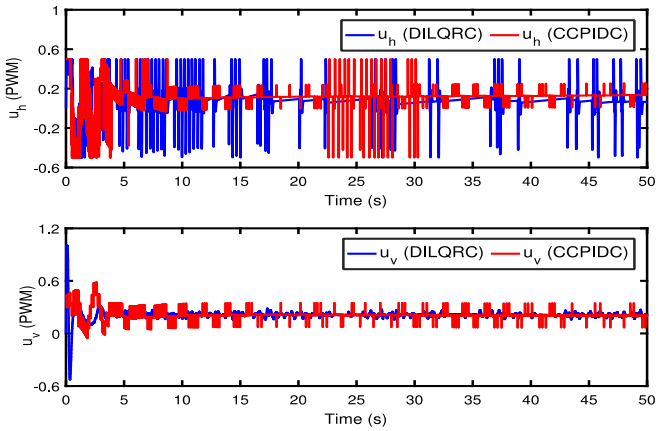

Fig. 8. Control signal of DILQRC and CCPIDC due to step input.

Figure 9 shows the response of the TRAS system due to square wave input with amplitude of 0.8 rad and frequency of 0.025 Hz in the horizontal plane and square wave input with an amplitude of 0.3 rad and frequency of 0.03Hz in the vertical plane with both DILQRC and CCPIDC. It can be clearly observed that the DILQRC accurately tracks the reference signal in both planes with a reduced number of oscillations in the vertical plane as compared to the CCPIDC. The improvement in

the DILQRC response for the vertical plane is achieved by means of the slower vertical observer poles, which are placed to attenuate disturbances and measurement noise signals.

Figure 10 shows the input control signals of DILQRC and CCPIDC due to the square wave input. Error, control and total variation indices for DILQRC and CCPIDC due to square wave input signal are summarised in Table 6. It can be observed that the DILQRC requires less control effort with less aggressive changes in the control signal to stabilise the horizontal plane as compared to CCPIDC. For the vertical plane, the DILQRC requires higher control effort to stabilise the system with less aggressive changes in the control signal as compared to CCPIDC. In terms of error index, the DILQRC achieves better performance by maintaining accurate tracking for the reference signals by reducing the error index by 28.57% and 24.40% for horizontal and vertical planes, respectively as compared to the CCPIDC.

In addition, it can be noticed that the CCPIDC produces high-frequency control signals due to the presence of the derivative parts of the controller [21], which are well known to amplify the measurement noise signals that lead to more variations and aggressive changes in the control signals [19, 35]. Whilst, the DILQRC does not contain any derivative parts. This, however, as expected, provides less aggressive and smooth control signals.

Table 6. Error, control and total variation indices of DILQR and CCPIDC due to square wave input.

Controller	Plane	IAE	IAC	TV
Pandey et al. [13]	Horizontal	15.76	25.09	2050.10
CCPIDC	Vertical	10.49	24.64	725.29
DILQRC	Horizontal	11.25	22.66	756.96
	Vertical	7.93	25.15	66.44

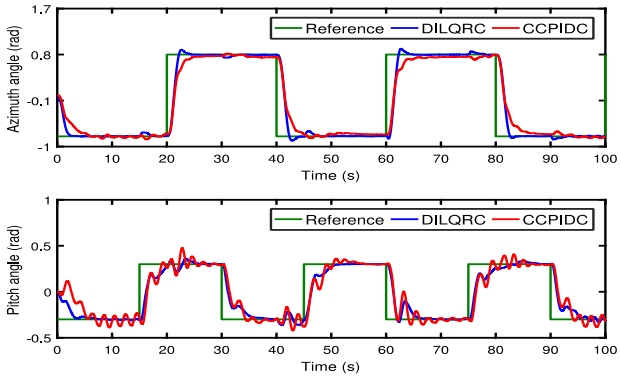

Fig. 9. Square-wave response of TRAS with DILQRC and CCPIDC.

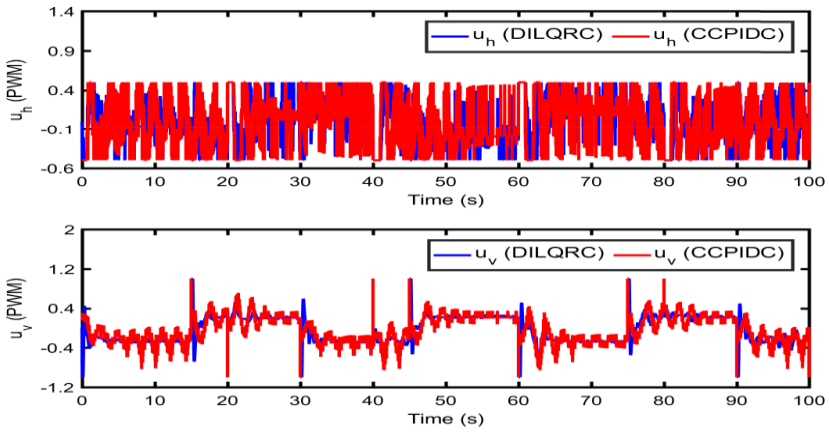

Fig. 10. Control signal of DILQRC and CCPIDC due square wave input.

8.2. Disturbance rejection

With the presence of environmental disturbances on real laboratory TRAS system, an external step input disturbance of 0.2 rad is injected in both planes of the system at a time (t = 25 s). The performance of DILQRC and CCPIDC is recorded and compared as shown in Fig. 11. It can be noticed that the DILQRC rejects the disturbances very fast and maintains accurate tracking for the set point in both planes as compared to the CCPIDC.

Figure 12 shows the input control signals of DILQRC and CCPIDC due to step input subjected to external disturbance. Table 7 summaries the error, control and total variation indices of DILQRC and CCPIDC subjected to external disturbance. It can be observed that the DILQRC requires higher control effort to stabilise both planes of the system with less aggressive changes in the control signals as compared to CCPIDC. In terms of error index, the DILQRC achieves better performance by rejecting the disturbances very fast and maintains accurate tracking for the reference signals by minimising the error index by 47.27% and 34.35% for horizontal and vertical planes, respectively as compared to the CCPIDC.

The fluctuations that happen in the response of the DILQRC (especially in the vertical plane) after the disturbances are injected at a time (t = 25 s), have occurred because the DILQRC reaches the limitations of the horizontal and vertical motors, as it can be clearly seen from the control signals in Fig. 12 at time (t = 25 s). However, this causes integral windup phenomena to happen, which directly activates the anti-integral windup compensators that quickly bring the control signals into the effective range before the performance of the DILQRC significantly degraded.

After the elimination of the injected disturbances, the response of the DILQRC shows small fluctuations in the vertical plane this is, however, because of the vibrations, which occur due to the vertical rotor load and motor torque [30].

Table 7. Error, control and total variation indices of DILQRC and CCPIDC due to step input subjected to external disturbance.

Controller	Plane	IAE	IAC	TV
Pandey et al. [13] CCPIDC	Horizontal	2.20	7.49	416.03
	Vertical	1.31	8.22	126.60
DILQRC	Horizontal	1.16	8.60	199.71
	Vertical	0.86	9.37	21.81

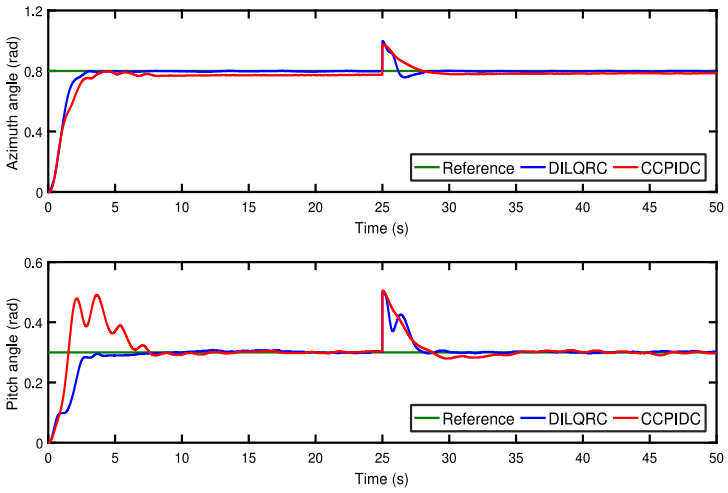

Fig. 11. Step input response of TRAS with DILQRC and CCPIDC subjected to external disturbance.

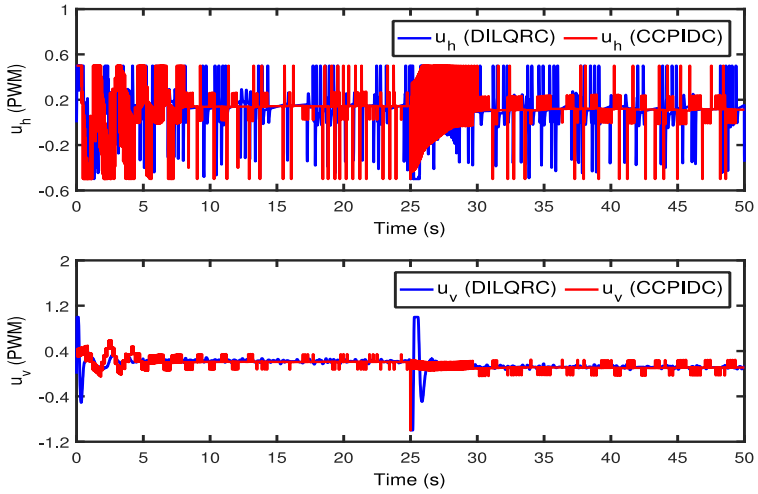

Fig. 12. Control signal of DILQRC and CCPIDC due to step input subjected to external disturbance.

9. Conclusions

In this work, control and stabilisation of real TRAS system in 2-DOF motion is successfully achieved. Decoupled integral LQR controller combined with full state observer and anti-integral windup compensator based on back-calculation technique has been described in this paper. Experimental results show that the DILQRC has a better transient and steady-state responses with magnificent reduction of settling time, overshoot percentage and error index. In all the experiments, the DILQRC produces smooth control signals with less aggressive changes as compared to the CCPIDC, furthermore, the settling time for the system is less than 2.61 seconds for both angles, which is considered as the fastest settling time as compared to the other controller design techniques presented in the literature. Overall, the DILQRC has the ability to maintain accurate tracking for the reference signals with fast disturbances rejection as compared to the existing CCPIDC tuned by the manufacturer.

Acknowledgement

The authors would like to acknowledge the UTM-GUP Grant from Universiti Teknologi Malaysia (UTM) and the Malaysian Government with vote number 17H40 for supporting this work.

Nomenclatures

A_1	Mechanical constant
B_1	Mechanical constant
C_1	Mechanical constant
a_1	Mechanical constant
a_2	Mechanical constant
c_1	Personal acceleration coefficient
c_2	Social acceleration coefficient
e	Error signal
e_h	Horizontal error signal
e_v	Vertical error signal
F	Particle swam optimisation cost function
f	Differential equation of each state
$F_h(x_3)$	Nonlinear relationship between the rotational speed of tail rotor and horizontal thrust
$F_v(x_6)$	Nonlinear relationship between the rotational speed of main rotor and vertical thrust
g	Gravitational acceleration, ms^{-2}
I_h	Moment of inertia for tail rotor, kgm^2
I_v	Moment of inertia for main rotor, kgm^2
J	Quadratic performance index function
J_h	Moment of inertia with respect to vertical axis, kgm^2
J_v	Moment of inertia with respect to horizontal axis, kgm^2
K	Linear optimal feedback matrix
K_e	Integral action gain
K_h	Linear optimal horizontal feedback matrix
K_v	Linear optimal vertical feedback matrix

K_{eh}	Horizontal integral action gain
K_{ev}	Vertical integral action gain
k_h	Friction constant of tail propeller
k_v	Friction constant of main propeller
L	Observer gain
l_m	Length of the main rotor, m
l_t	Length of the tail rotor, m
n_s	Number of samples
P	Solution of Riccati equation
Q	Positive semi-definite matrix
R	Square positive definite matrix
r	Reference signal
r_1	Randomly distributed number between 0 and 1
r_2	Randomly distributed number between 0 and 1
r_h	Horizontal reference signal
r_v	Vertical reference signal
u	Input vector
$\overline{u}$	Saturated control signal
u_h	Control input to tail rotor
$\overline{u}_h$	Saturated horizontal control signal
$u_h(x_3)$	Nonlinear relationship between rotational speed of tail rotor and the control input to the tail rotor
u_{max}	Maximum control signal
u_{min}	Minimum control signal
u_v	Control input to the main rotor
$\overline{u}_v$	Saturated vertical control signal
$u_v(x_6)$	Nonlinear relationship between the rotational speed of main rotor and the control input to main rotor
v_i	Velocity vector
w	Inertia weight factor
w_{damp}	Damping ratio of inertia coefficient
x	State vector
$\hat{x}$	Estimated state
x_1	Azimuth angle, rad(
x_2	Azimuth angular velocity, rad/s
x_3	Rotational speed of the tail rotor, rad/s
x_4	Pitch angle, rad
x_5	Pitch angular velocity, rad/s
x_6	Rotational speed of main rotor, rad/s
x_a	Integral action state
x_{ah}	Horizontal integral action state
x_{av}	Vertical integral action state
x_{GB}	Global best
x_i	Position vector
x_{PB}	Personal best
y	Output vector
y_h	Horizontal output vector
y_v	Vertical output vector

Abbreviations

CCPIDC	Cross Coupled PID Controller
DILQRC	Decoupled Integral LQR Controller
DOF	Degree of Freedom
IAC	Integrated Absolute Control
IAE	Integrated Absolute Error
LQR	Linear Quadratic Regulator
MIMO	Multi Input Multi Output
MPC	Model Predictive Control
OV	Overshoot
PID	Proportional Integral Derivative
PSO	Particle Swarm Optimization
RT	Rise Time
SISO	Single Input Single Output
ST	Settling Time
TRAS	Two Rotor Aero-dynamical System
TRMS	Twin Rotor MIMO System
TV	Total Variation

References

1. Seborg, D.E.; Edgar, T.F.; Mellichamp, D.A.; and Doyle, F.J. (2010). *Process dynamics and control* (3rd ed.). Hoboken, New Jersey: John Wiley & Sons, Inc.
2. Coughanowr, D.R.; and LeBlanc, S.T. (2008). *Process systems analysis and control* (3rd ed.). New York: McGraw-Hill Higher Education.
3. Chrif, L.; and Kadda, Z.M. (2014). Aircraft control system using LQG and LQR controller with optimal estimation-Kalman filter design. *Procedia Engineering*, 80, 245-257.
4. Juang, J.-G.; Huang, M.-T.; and Liu, W.-K. (2008). PID control using presearched genetic algorithms for a MIMO system. *IEEE Transactions on Systems*, Man and, Cybernetics, Part C, (Applications and Reviews), 38(5), 716-727.
5. Skogestad, S. (2003). Simple analytic rules for model reduction and PID controller tuning. *Journal of Process Control*, 13(4), 291-309.
6. Ijaz, S.; Hamayun, M.T.; Yan, L.; and Mumtaz, M.F. (2016). Fractional order modeling and control of twin rotor aero dynamical system using nelder mead optimization. *Journal of Electrical Engineering and Technology*, 11(6), 1863-1871.
7. Yang, X.; Cui, J.; Lao, D.; Li, D.; and Chen, J. (2016). Input shaping enhanced active disturbance rejection control for a twin rotor multi-input multi-output system (TRMS). *ISA Transactions*, 62, 287-298.
8. Ahmad, M.; Ali, A.; and Choudhry, M.A. (2016). Fixed-structure $H\infty$ controller design for two-rotor aerodynamical system (TRAS). *Arabian Journal for Science and Engineering*, 41(9), 3619-3630.
9. Al-Mahturi, A.; and Wahid, H. (2017). Optimal tuning of linear quadratic regulator controller using a particle swarm optimization for two-rotor

aerodynamical system. *International Journal of Electronics and Communication Engineering*, 11(2), 196-202.

10. Phillips, A.; and Sahin, F. (2014). Optimal control of a twin rotor MIMO system using LQR with integral action. *Proceedings of the World Automation Congress (WAC)*. Waikoloa, Hawaii, 114-119.
11. Pandey, S.K.; and Laxmi, V. (2015). Optimal control of twin rotor MIMO system using LQR technique. *Computational Intelligence in Data Mining*, 1, 11-21.
12. Wen, P.; and Lu, T.-W. (2008). Decoupling control of a twin rotor MIMO system using robust deadbeat control technique. *IET Control Theory and Applications*, 2(11), 999-1007.
13. Pandey, V.K.; Kar, I.; and Mahanta, C. (2017). Controller design for a class of nonlinear MIMO coupled system using multiple models and second level adaptation. *ISA Transactions*, 69, 256-272.
14. Butt, S.S.; and Aschemann, H. (2015). Multi-variable integral sliding mode control of a two degrees of freedom helicopter. *IFAC-PapersOnLine*, 48(1), 802-807.
15. Duţescu, D.-A.; Radac, M.-B.; and Precup, R.-E. (2017). Model predictive control of a nonlinear laboratory twin rotor aero-dynamical system. *Proceedings of the 15th International Symposium on Applied Machine Intelligence and Informatics (SAMI)*. Herl'any, Slovakia, 37-42.
16. Raghavan, R.; and Thomas, S. (2016). MIMO model predictive controller design for a twin rotor aerodynamic system. *Proceedings of the IEEE International Conference on Industrial Technology (ICIT)*. Taipei, Taiwan, 96-100.
17. Raptis, I.A.; and Valavanis, K.P. (2011). *Linear and nonlinear control of small-scale unmanned helicopters* (1st ed.). Dordrecht: Springer Netherlands.
18. Haruna, A.; Mohamed, Z.; Efe, M.O.; and Basri, M.A.M. (2017). Dual boundary conditional integral backstepping control of a twin rotor MIMO system. *Journal of the Franklin Institute*, 354(15), 6831-6854.
19. Astrom, K.J.; and Hagglund, T. (2006). *Advanced PID control*. Research Triangle Park, North Carolina: The Instrumentation, Systems, and Automation (ISA) Society .
20. Shin, H.-B.; and Park, J.-G. (2012). Anti-windup PID controller with integral state predictor for variable-speed motor drives. *IEEE Transactions on Industrial Electronics*, 59(3), 1509-1516.
21. INTECO. (2013). Two rotor aero-dynamical system. *User's Manual*. Krakaw, Poland: INTECO Ltd.
22. Rahideh, A.; and Shaheed, M.H. (2007). Mathematical dynamic modelling of a twin-rotor multiple input-multiple output system. *Proceedings of the Institution of Mechanical Engineers. Part 1: Journal of Systems and Control Engineering*, 221(1), 89-101.
23. Rahideh, A.; Shaheed, M.H.; and Huijberts, H.J.C. (2008). Dynamic modelling of a TRMS using analytical and empirical approaches. *Control Engineering Practice*, 16(3), 241-259.

24. Tastemirov, A.; Lecchini-Visintini, A.; and Morales-Viviescas, R.M. (2017). Complete dynamic model of the twin rotor MIMO system (TRMS) with experimental validation. *Control Engineering Practice*, 66, 89-98.
25. Khalil, H.K. (2002). *Nonlinear systems* (3rd ed.). Essex, England: Pearson Education Limited.
26. Nise, N.S. (2011). *Control systems engineering* (6th ed.). Hoboken, New Jersey: John Wiley & Sons, Inc.
27. Kumar, E.V.; Raaja, G.S.; and Jerome, J. (2016). Adaptive PSO for optimal LQR tracking control of 2 DoF laboratory helicopter. *Applied Soft Computing*, 41, 77-90.
28. Hamidi, J. (2012). Control system design using particle swarm optimization (PSO*). International Journal of Soft Computing and Engineering (IJSCE)*, 1(6), 116-119.
29. Ogata, K. (2010). *Modern control engineering* (5th ed.). Upper Saddle River, New Jersey: Prentice Hall.
30. Ahmad, S.M.; Chipperfield, A.J.; and Tokhi, O. (2000). Dynamic modeling and optimal control of a twin rotor MIMO system. *Proceedings of the IEEE 2000 National Aerospace and Electronics Conference*. Dayton, Ohio, 391-398.
31. Visioli, A. (2006). *Practical PID control* (1st ed.). London: Springer-Verlag.
32. Choi, J.-W.; and Lee, S.-C. (2009). Antiwindup strategy for PI-type speed controller. *IEEE Transactions on Industrial Electronics*, 56(6), 2039-2046.
33. Astrom, K.J.; and Rundqwist, L. (1989). Integrator windup and how to avoid it. *American Control Conference*. Pittsburgh, Pennsylvania, 1693-1698.
34. Pawlowski, A.; Rodriguez, C.; Guzman, J.L.; Berenguel, M.; and Dormido, S. (2016). Measurable disturbances compensation: Analysis and tuning of feedforward techniques for dead-time processes. *Processes*, 4(2), 12.
35. Knospe, C. (2006). PID control. *IEEE Control Systems Magazine*, 26(1), 30-31.